Supplementary Information

Bioinspired Gel Polymer Electrolyte for Wide Temperature Lithium Metal Battery

Shuohan Liu,[1] Wensheng Tian,[2] Jieqing Shen,[1] Zhikai Wang,[1] Hui Pan,[1*] Xuchen Kuang,[1] Cheng Yang,[2*] Shunwei Chen,[3] Xiujun Han,[3*] Hengdao Quan,[4] and Shenmin Zhu[1*]

[1]State Key Laboratory of Metal Matrix Composites, School of Materials Science and Engineering, Shanghai Jiao Tong University, Shanghai 200240, China
[2]State Key Laboratory of Space Power-Sources, Shanghai Institute of Space Power-Sources, Shanghai 200245, China
[3]School of Materials Science and Engineering, Qilu University of Technology (Shandong Academy of Sciences), Jinan, Shandong 250353, China
[4]School of Chemistry and Chemical Engineering, Beijing Institute of Technology, 5 South Zhongguancun Street, Beijing 100081, China

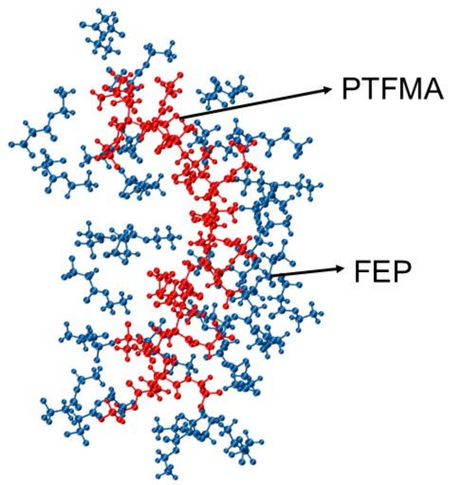

Supplementary Figure 1. Snapshots of WSGPE partial MD simulations. FEP in blue and PTFMA in red.

Supplementary Figure 2. Optical photograph of WSGPE electrolyte. WSGPE is a homogeneous transparent gel.

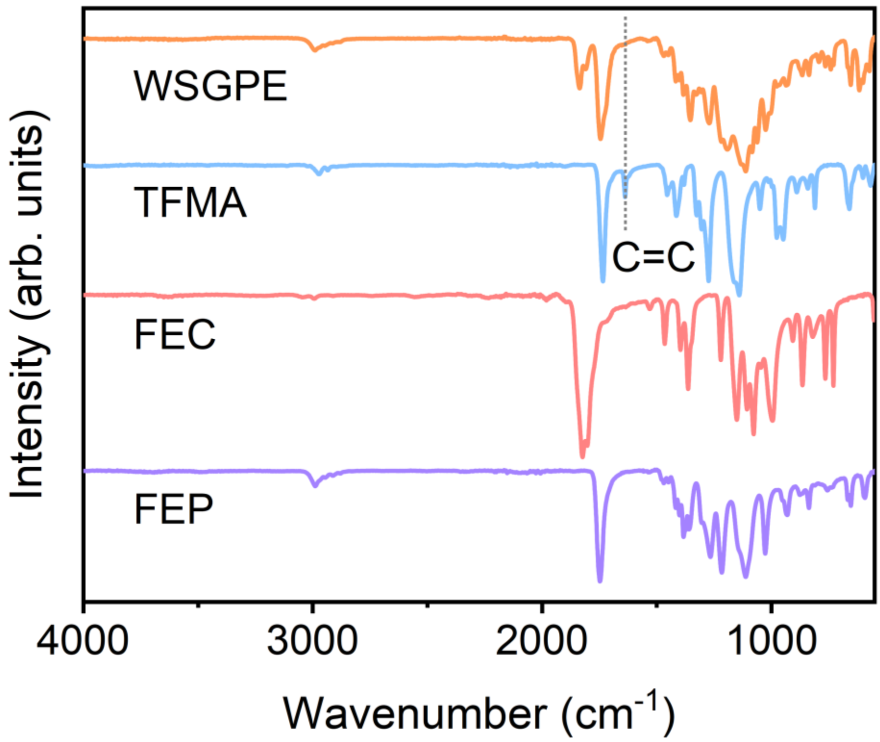

Supplementary Figure 3. FTIR spectra of WSGPE and its components. FTIR spectra of FEP, FEC, TFMA and WSGPE.

Supplementary Table 1. DFT results of WSGPE. Binding energy between components in WSGPE calculated by DFT.

Component A	Component B	Binding energy (kJ/mol)
$TFSI^{-}$	FEC	2727.87
$TFSI^{-}$	FEP	15645.06
$TFSI^{-}$	PTFMA	3346.05
PTFMA	FEC	7975.83
PTFMA	FEP	29380.90

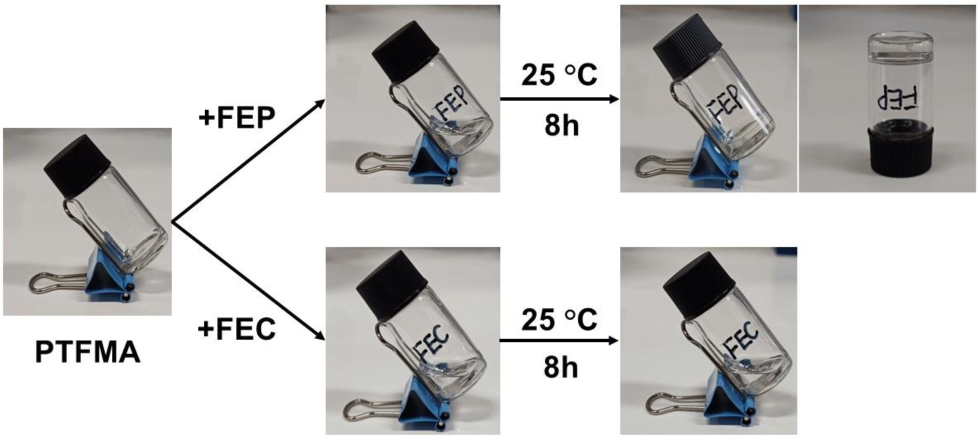

Supplementary Figure 4. The static experiment of different components. The diagram of static experiment at 25 °C.

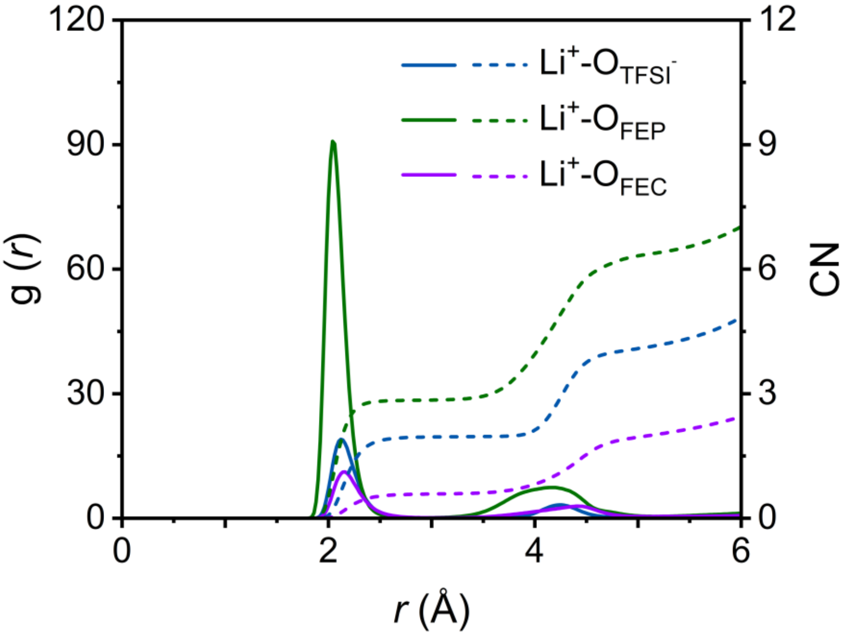

Supplementary Figure 5. The solvation structure of liquid electrolyte. RDFs and CNs of Li^+ in the liquid electrolyte.

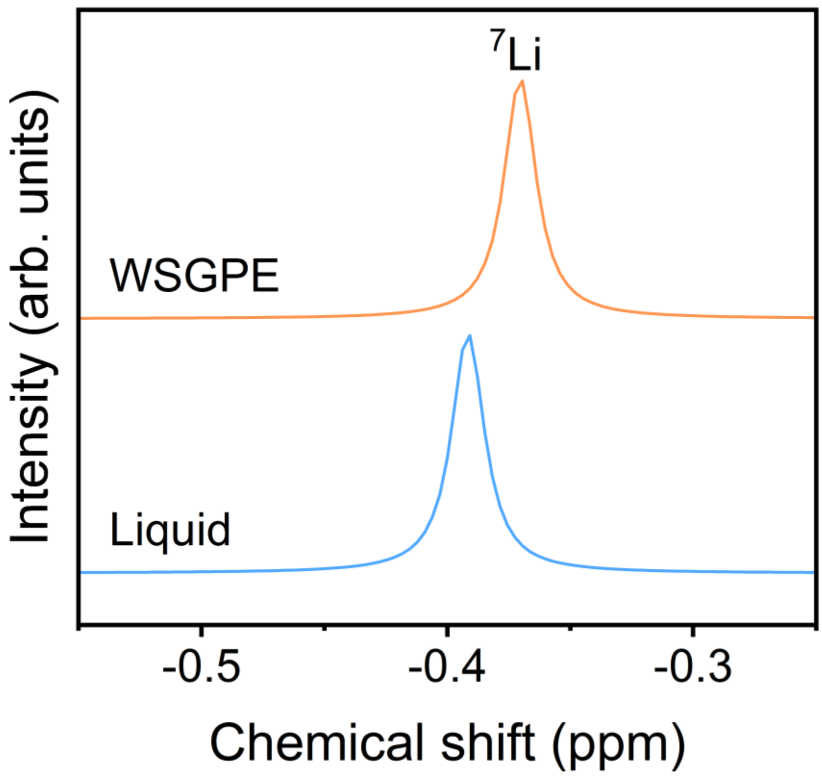

Supplementary Figure 6. Li^+ solvation structures in different electrolytes. ^{7}Li NMR of liquid electrolyte and WSGPE.

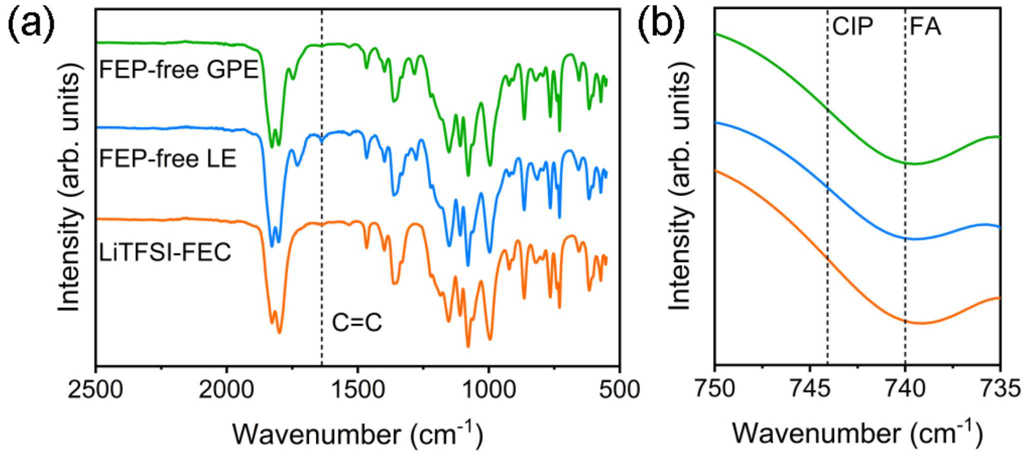

Supplementary Figure 7. FTIR spectra of different electrolytes. (**a**) FTIR spectra and (**b**) S−N−S stretching of $TFSI^-$ of FEC liquid electrolyte, FEP-free LE and FEP-free GPE, respectively.

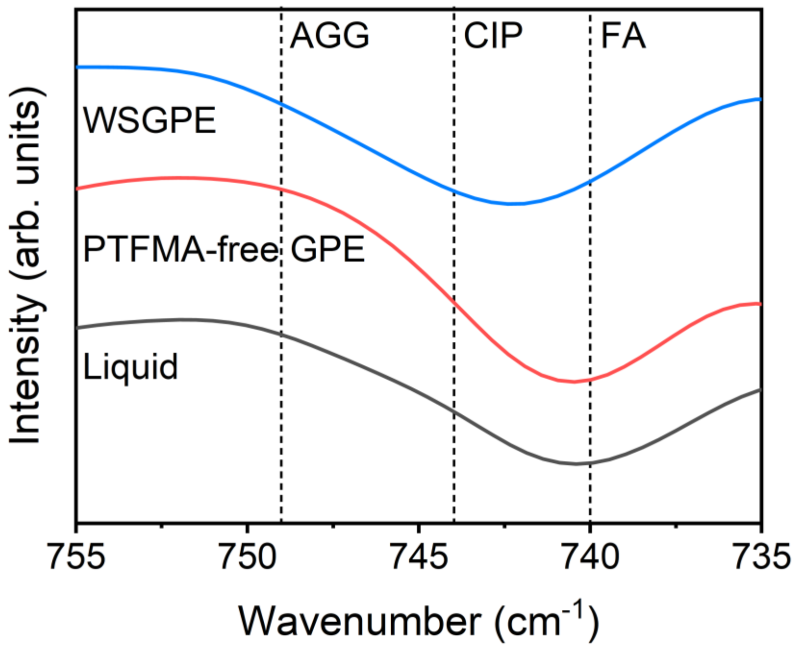

Supplementary Figure 8. FTIR spectra of different electrolytes. FTIR spectra of liquid electrolyte, PTFMA-free GPE and WSGPE.

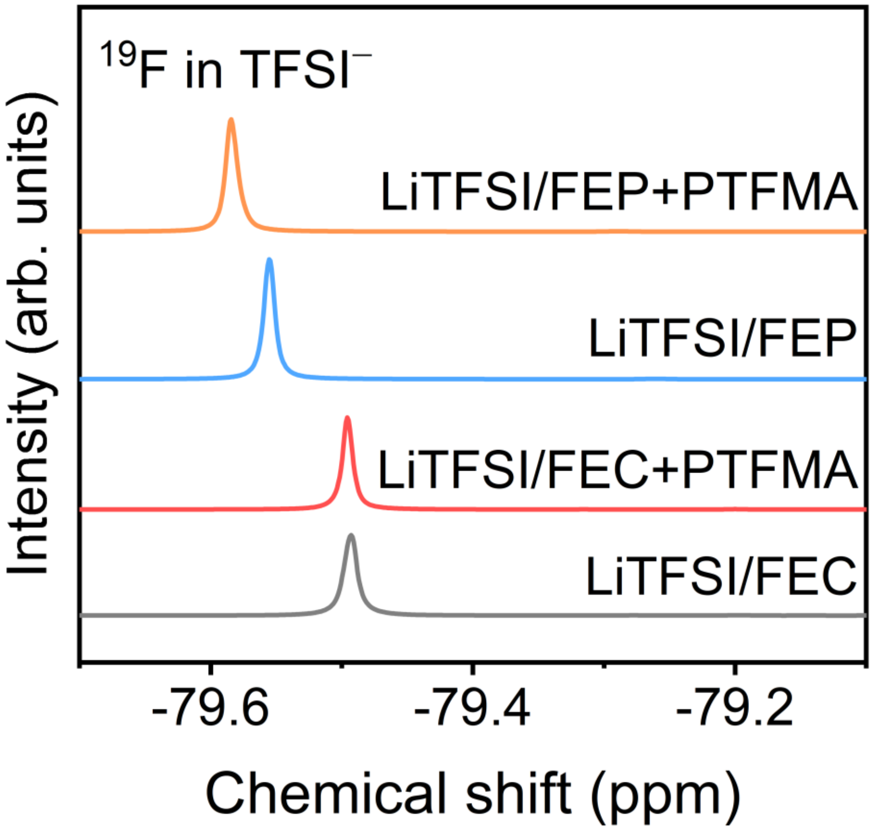

Supplementary Figure 9. Interactions between different components. ^{19}F NMR of $TFSI^{-}$.

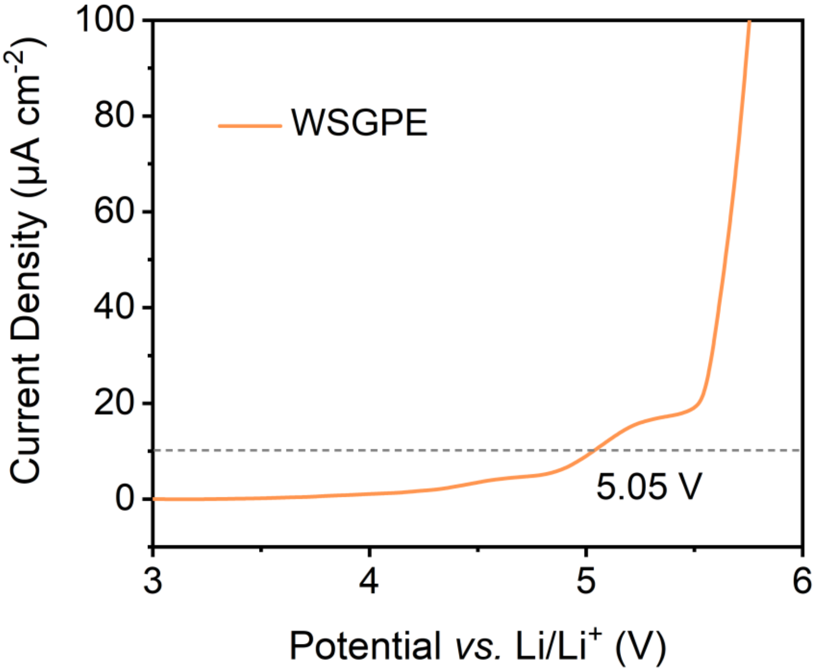

Supplementary Figure 10. The electrochemical window of WSGPE. LSV curve of WSGPE at 25 °C.

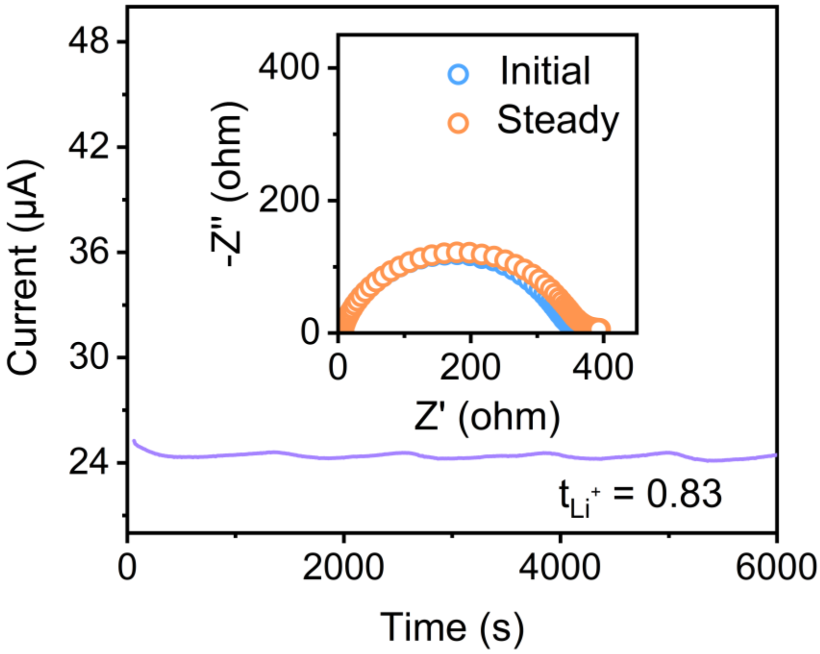

Supplementary Figure 11. Li^+ transference number of WSGPE at 25 °C. Current variation with polarization of the Li|WSGPE|Li symmetrical cell. Inset: Nyquist curves before and after polarization.

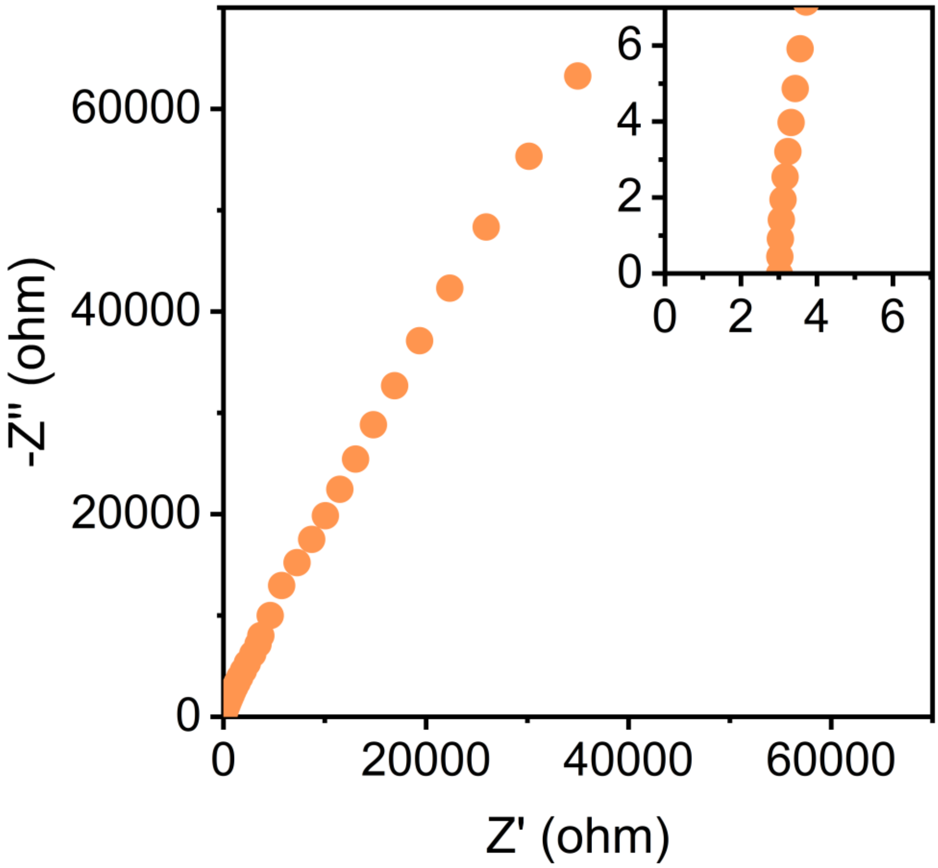

Supplementary Figure 12. Nyquist curve of the SS|WSGPE|SS. The ionic conductivity of WSGPE is 4.40×10^{-4} S cm^{-1} at 25 °C.

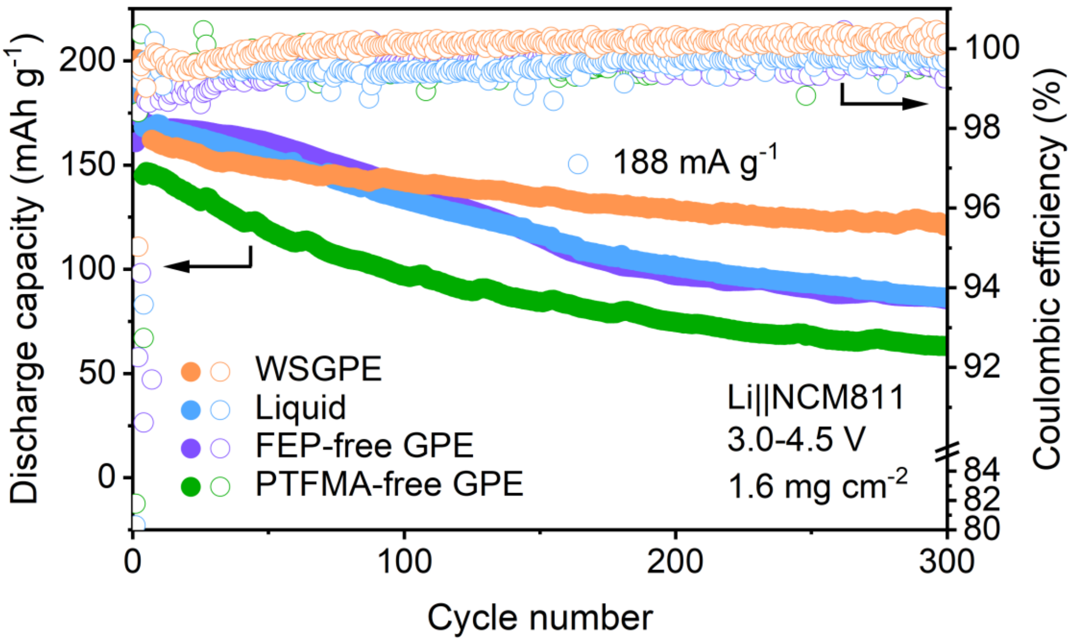

Supplementary Figure 13. Electrochemical performance of Li||NCM811 cells using different electrolytes. Cycling performance of Li||NCM811 cells using different electrolytes at 188 mA g^{-1} between 3−4.5 V.

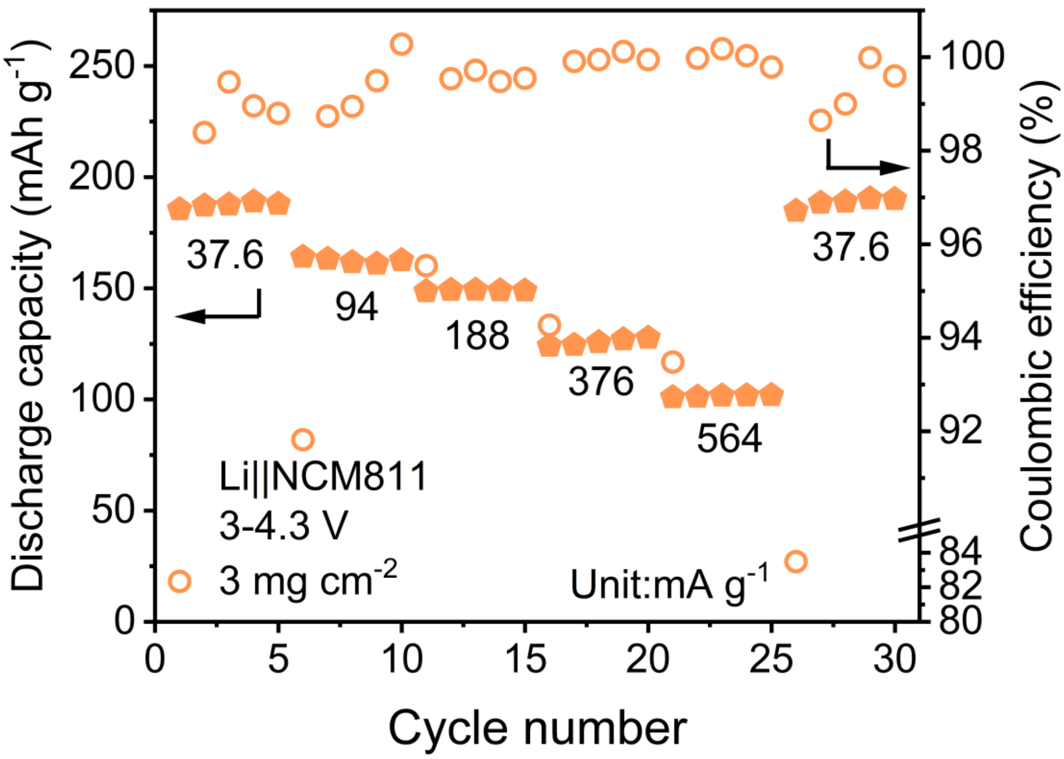

Supplementary Figure 14. Electrochemical performance of Li||NCM811 cells.

Rate performance of Li|WSGPE|NCM811.

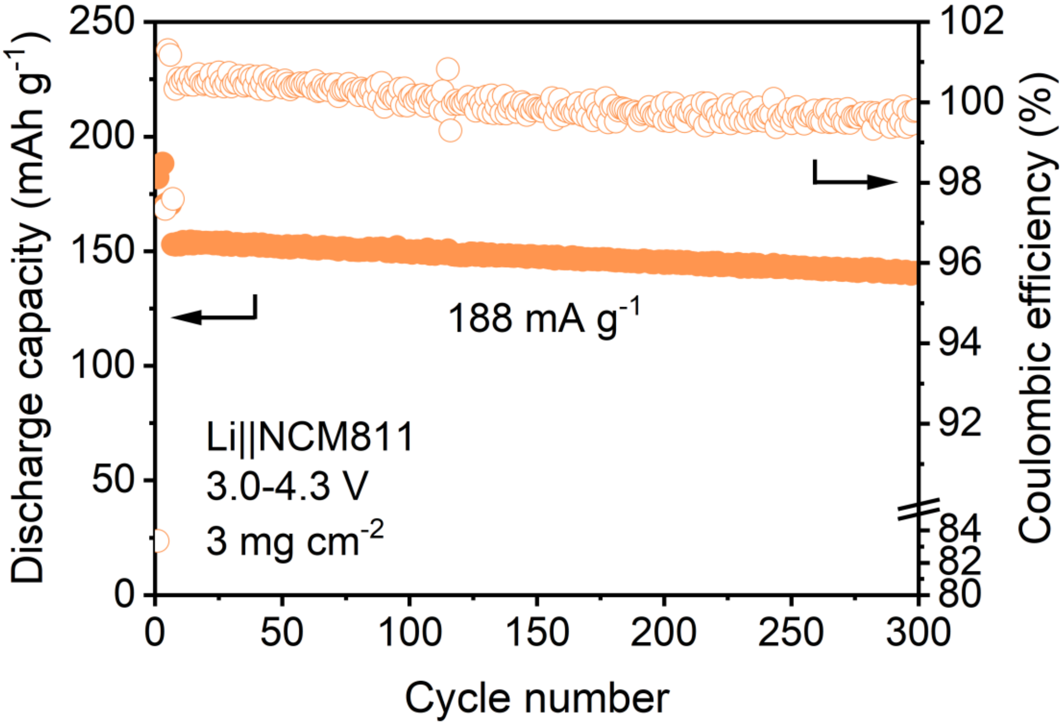

Supplementary Figure 15. Electrochemical performance of Li||NCM811 cells. Cycling performance of Li|WSGPE|NCM811 with medium mass loading of 3 mg cm^{-2} at 188 mA g^{-1}.

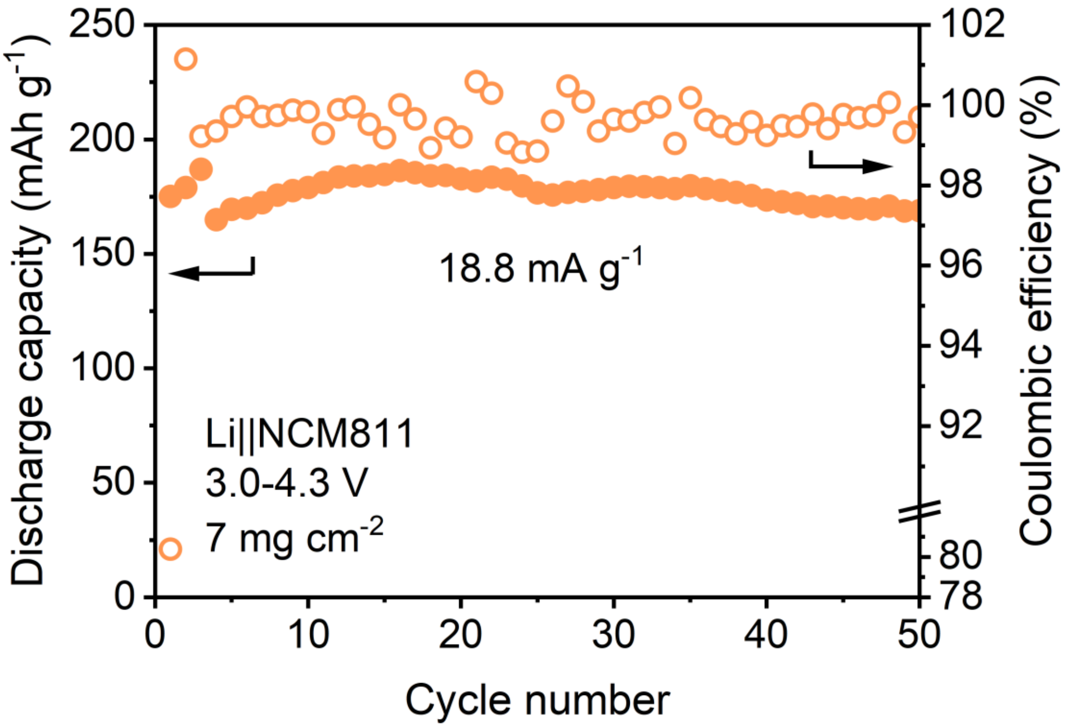

Supplementary Figure 16. Electrochemical performance of Li||NCM811 cells. Cycling performance of Li|WSGPE|NCM811 with a high mass loading of 7 mg cm^{-2}.

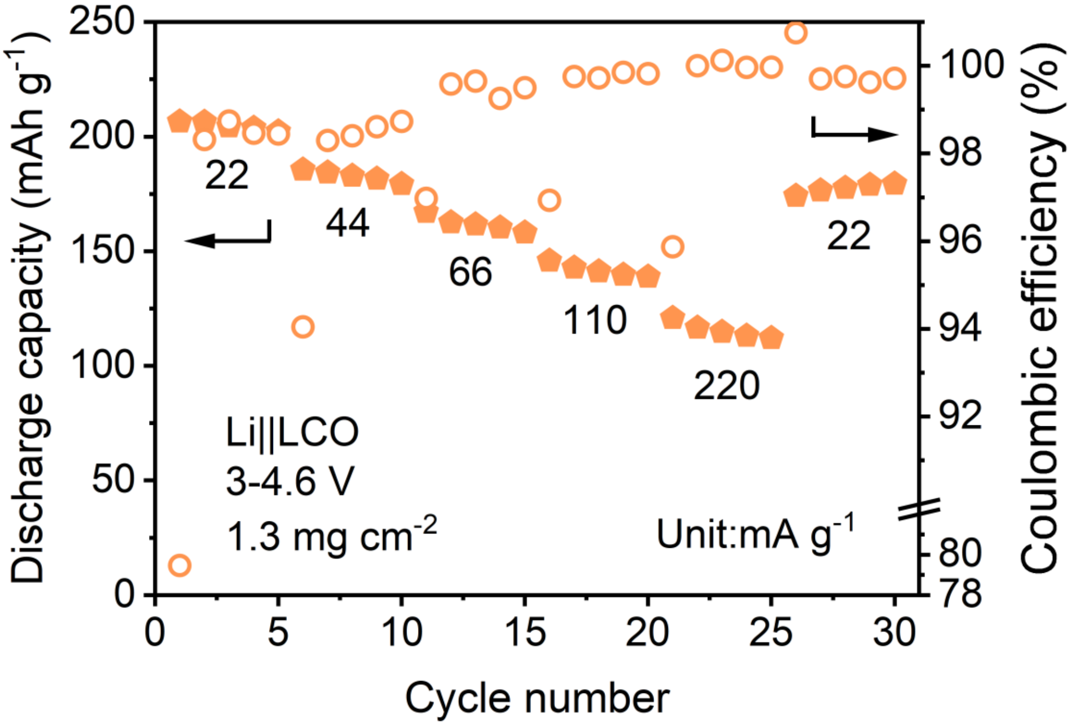

Supplementary Figure 17. Electrochemical performance of Li||LCO cells. Rate performance of Li|WSGPE|LCO.

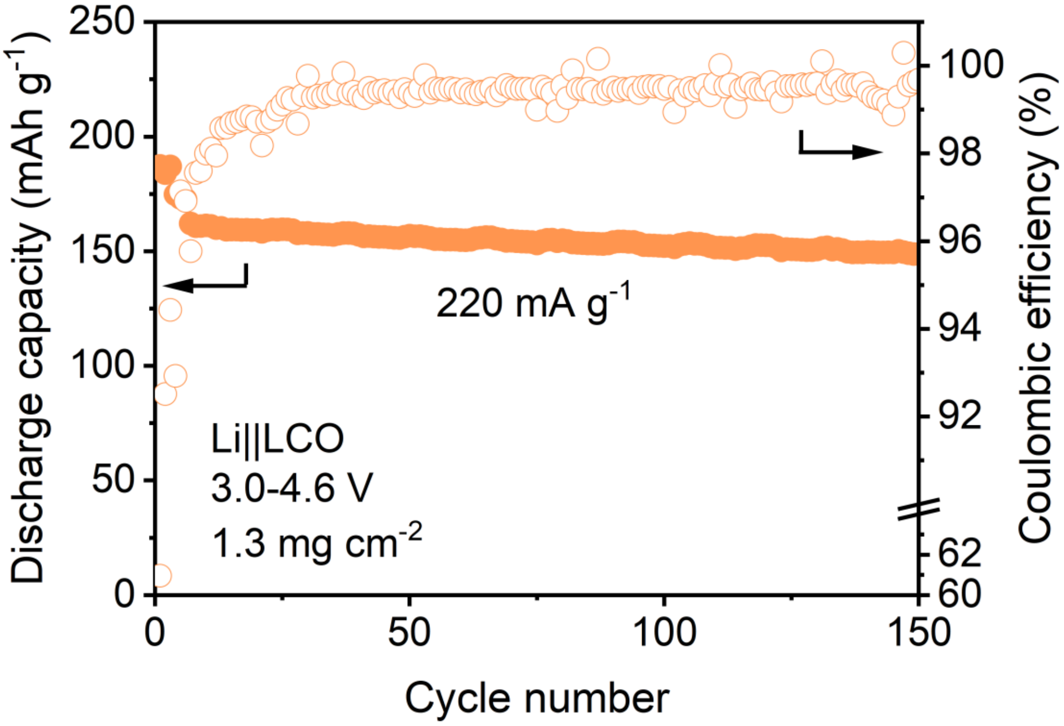

Supplementary Figure 18. Electrochemical performance of Li||LCO cells.

Cycling performance of Li|WSGPE|LCO at 220 mA g^{-1} between 3−4.6 V.

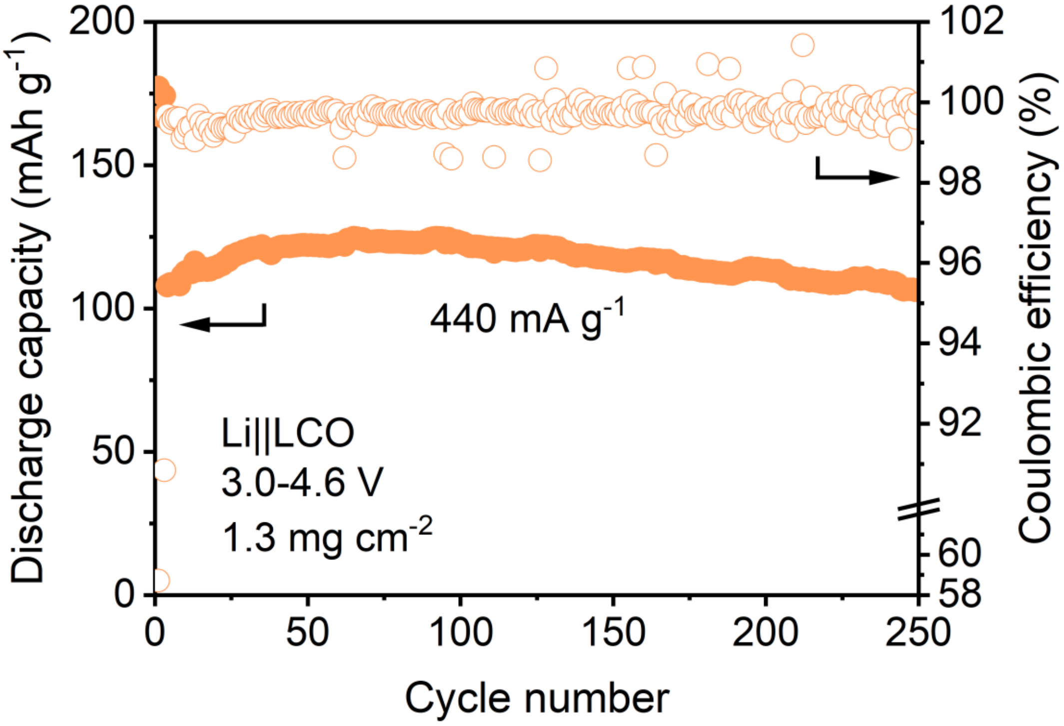

Supplementary Figure 19. Electrochemical performance of Li||LCO cells. Cycling performance of Li|WSGPE|LCO at 440 mA g^{-1} between 3−4.6 V.

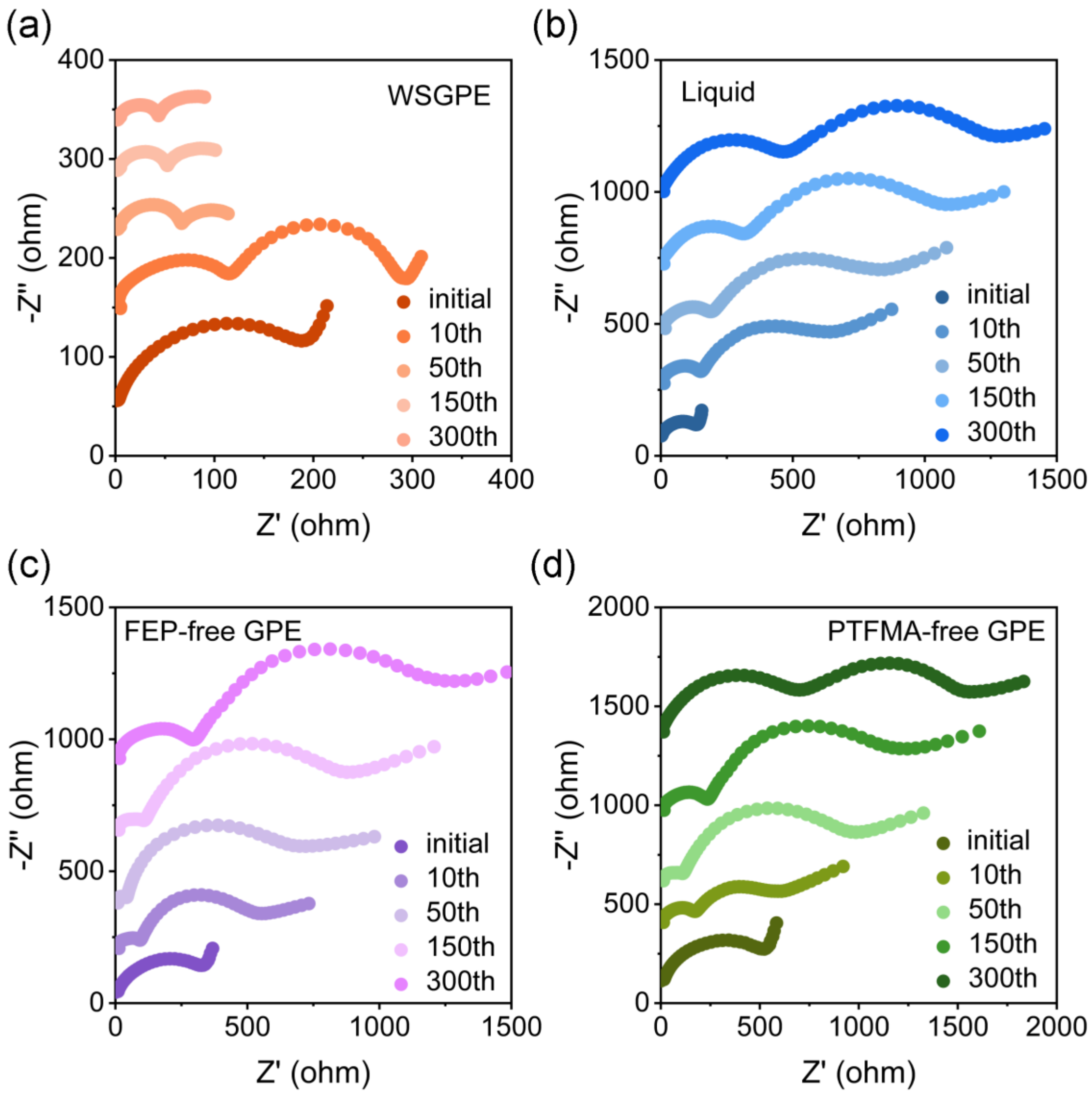

Supplementary Figure 20. EIS plots of Li||NCM811 cells with different electrolytes. EIS plots of Li||NCM811 cells using (**a**) WSGPE, (**b**) liquid electrolyte, (**c**) FEP-free GPE and (**d**) PTFMA-free GPE during cycling.

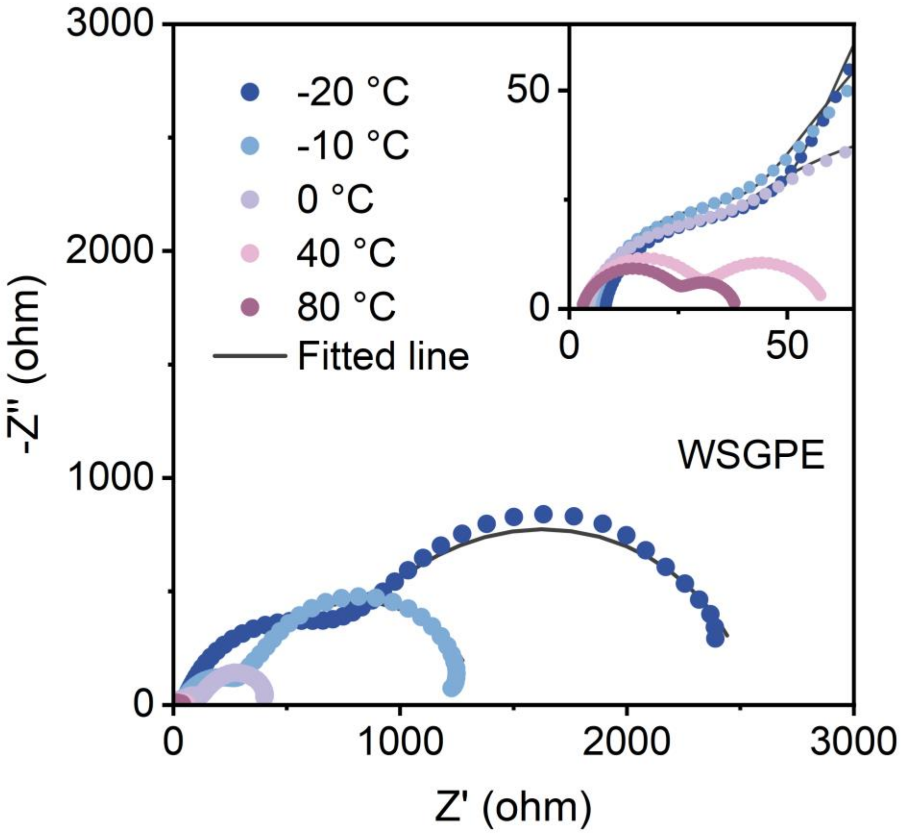

Supplementary Figure 21. EIS plots of WSGPE batteries. Nyquist impedance plots of Li|WSGPE|NCM811 cells at different temperatures after 10 cycles.

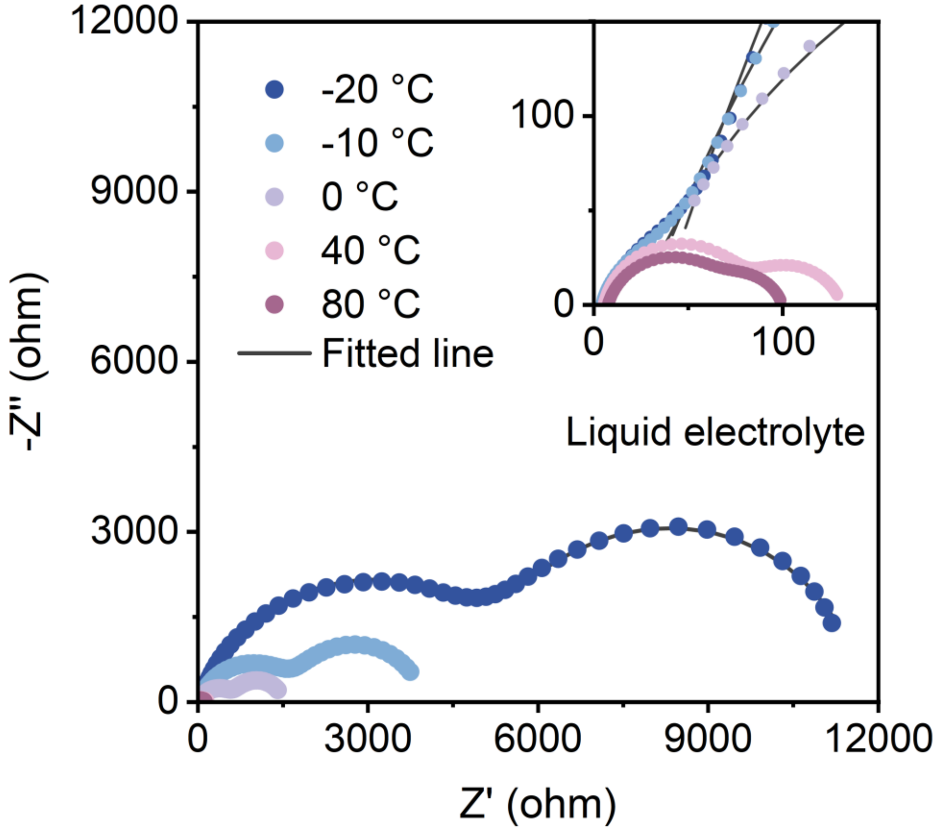

Supplementary Figure 22. EIS plots of liquid batteries. Nyquist impedance plots of Li|liquid electrolyte|NCM811 cells at different temperatures after 10 cycles.

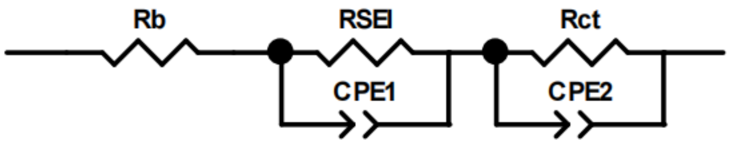

Supplementary Figure 23. The equivalent circuit diagram of EIS. The equivalent circuit diagram of EIS for Li||NCM811 cells.

Supplementary Table 2. EIS fitting results of Li||NCM811 cells. The impedance values of the WSGPE cell and the liquid cell at different temperatures.

	WSGPE				**Liquid electrolyte**			
	$R_{b}(\Omega)$	$R_{SEI}(\Omega)$	$R_{ct}(\Omega)$	**Error**	$R_{b}(\Omega)$	$R_{SEI}(\Omega)$	$R_{ct}(\Omega)$	**Error**
80 °C	2.2	22.7	12.7	0.16	2.7	60.2	32.2	0.18
40 °C	2.8	29.2	26.5	0.48	3.2	75.8	50.8	0.47
0 °C	4.5	123.4	295.8	0.20	5.7	651.4	814.5	0.12
-10 °C	5.3	303.0	1037	0.16	6.1	1802	2082	0.26
-20 °C	7.7	814.1	1728	0.13	8.5	5544	6132	0.22

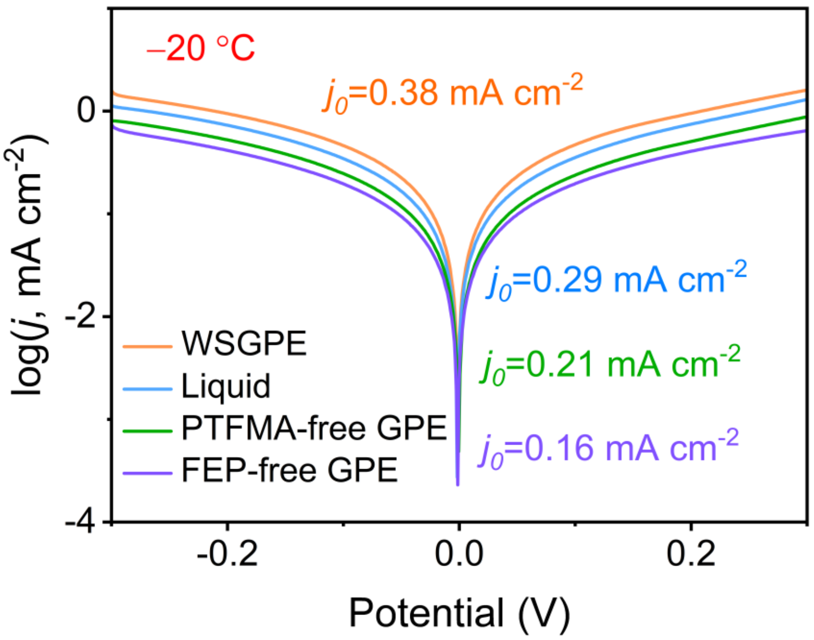

Supplementary Figure 24. Exchange current density of different electrolytes at LT. Tafel plots of Li plating/stripping in different electrolytes at −20 °C.

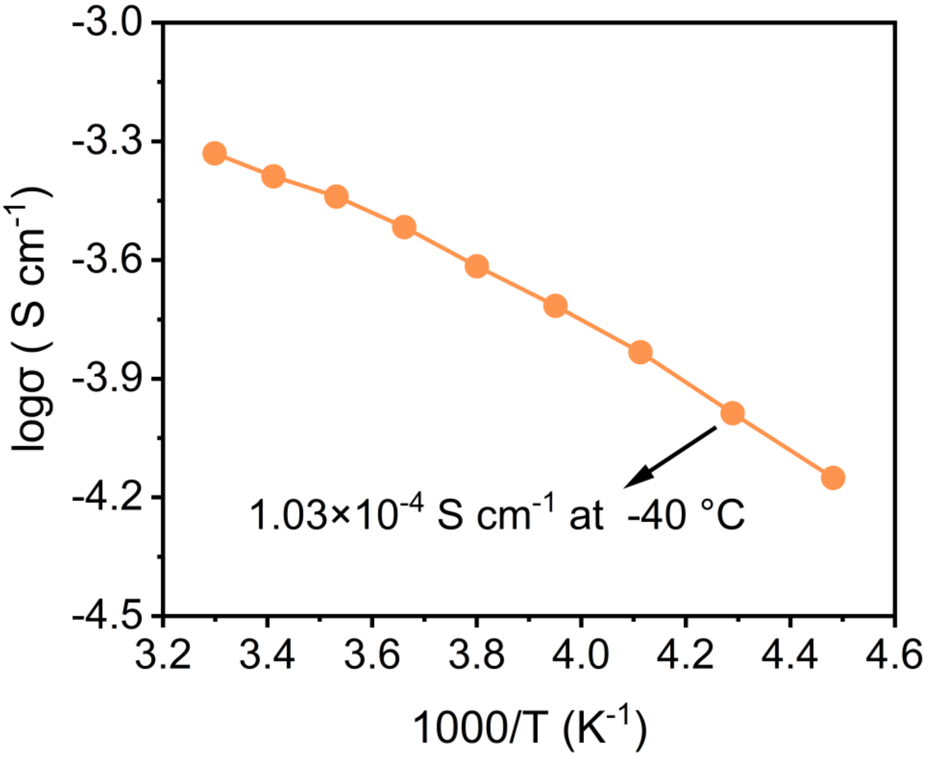

Supplementary Figure 25. Electrochemical performance of WSGPE at different temperatures. The curve of ionic conductivities with temperature of WSGPE.

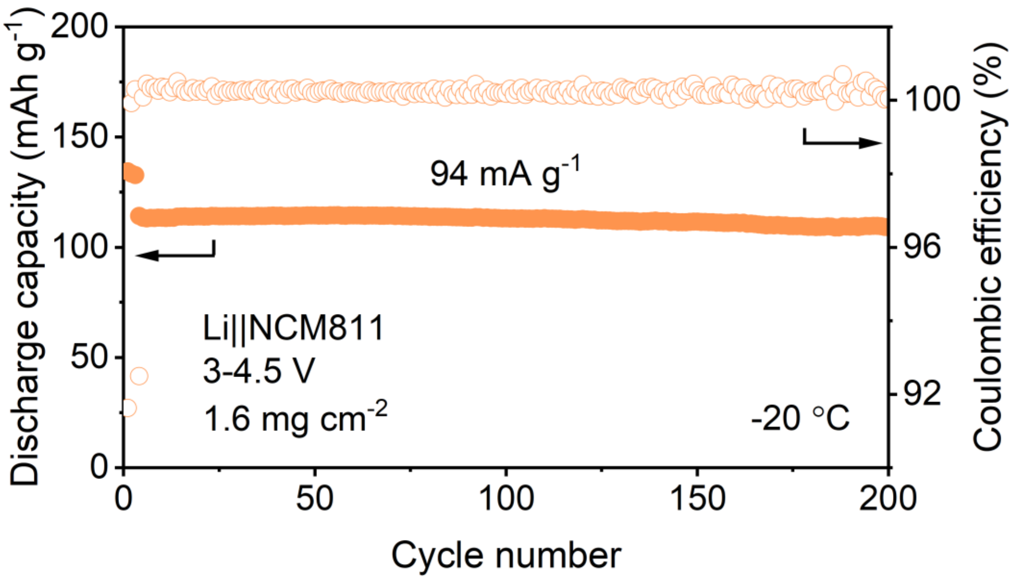

Supplementary Figure 26. Electrochemical performance at LT. Cycling performance of the Li|WSGPE|NCM811 cell at −20 °C and 94 mA g^{-1}.

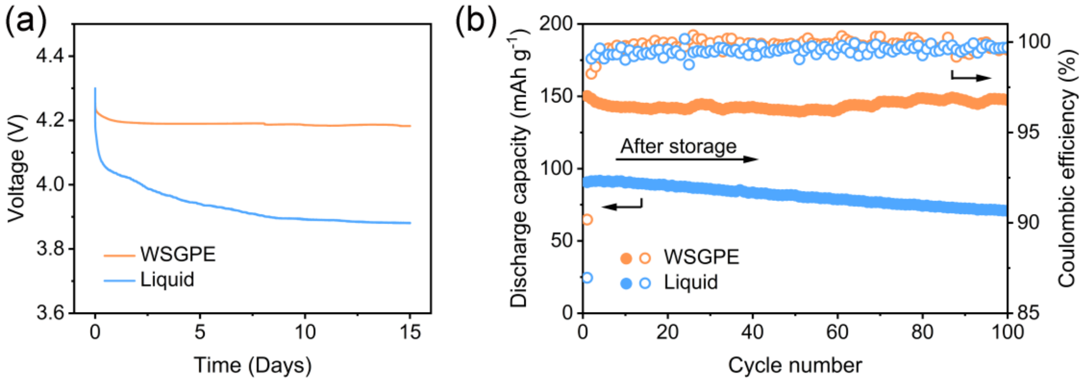

Supplementary Figure 27. The self-discharge performance. (**a**) Self-discharge curves of 4.3 V fully-charged Li||NCM811 cells for 15-day storage under 25 °C using various electrolytes. (**b**) Cycling performance at 188 mA g^{-1} after 15-day self-discharge storage.

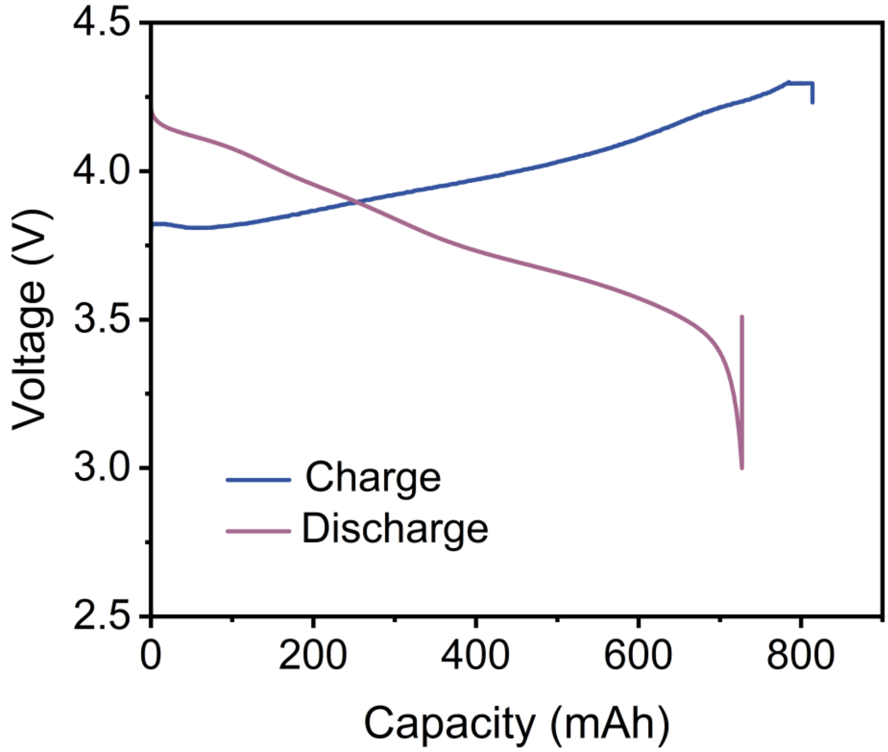

Supplementary Figure 28. The formation cycle of the 750 mAh pouch cell. Charge to 4.3 V at a constant current of 75 mA, followed by a constant-voltage charge for 30 minutes, and then discharge to 2.8 V at a constant current of 75 mA.

Supplementary Table 3. Parameters of the 750 mAh pouch cell. Parameters for calculation of the specific energy of the 750 mAh pouch cell.

	Parameters	Areal weight (mg cm^{-2})	Layers	Areal (cm^2)	Weight (mg)
Li	50 μm	2.67	3	40	320.4
NCM811	70 μm	23.4	2		3744
Separator	16 μm	1.32	4		211.2
Electrolyte	2 g Ah^{-1}				1500
Total weight (mg)					5775.6

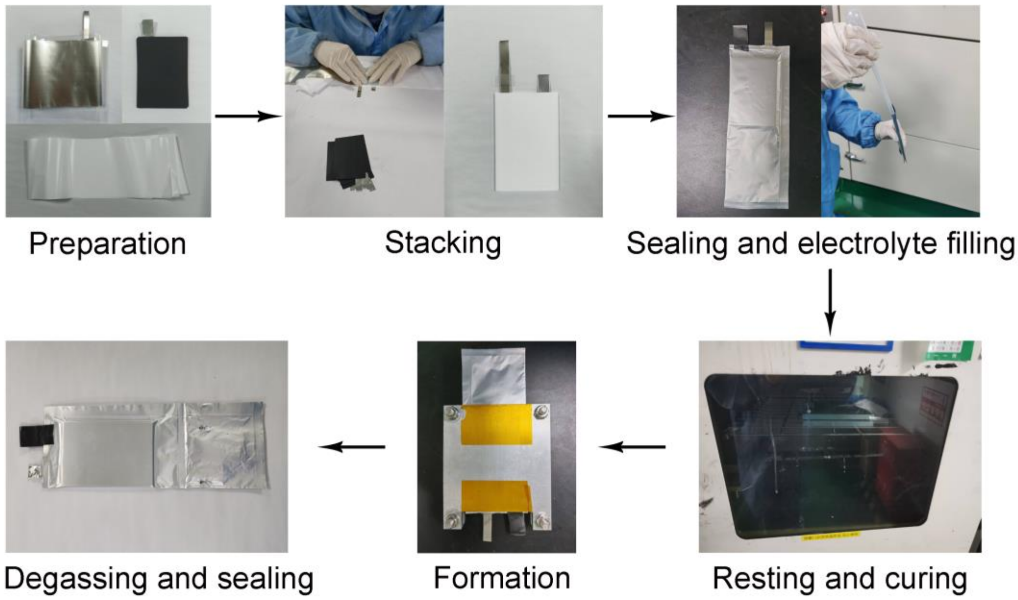

Supplementary Figure 29. Preparation process of the 5.4 Ah pouch cell. Diagram of the preparation process of the 5.4 Ah pouch cell.

Supplementary Table 4. Preparation of the 5.4 Ah pouch cell. Detailed preparation parameters for the 5.4 Ah pouch cell.

	Thickness (μm)	Areal weight (mg cm^{-2})	Layers	Size (cm×cm)
Li	50	2.67	15	5×8
NCM811	70	24.02	14	
Separator	16	1.32	16	
Electrolyte	2 g Ah^{-1}			
Total weight (g)	43.16			
Discharge capacity (Ah)	5.124			
Voltage (V)	3.8			
Specific energy (Wh kg^{-1})	451			

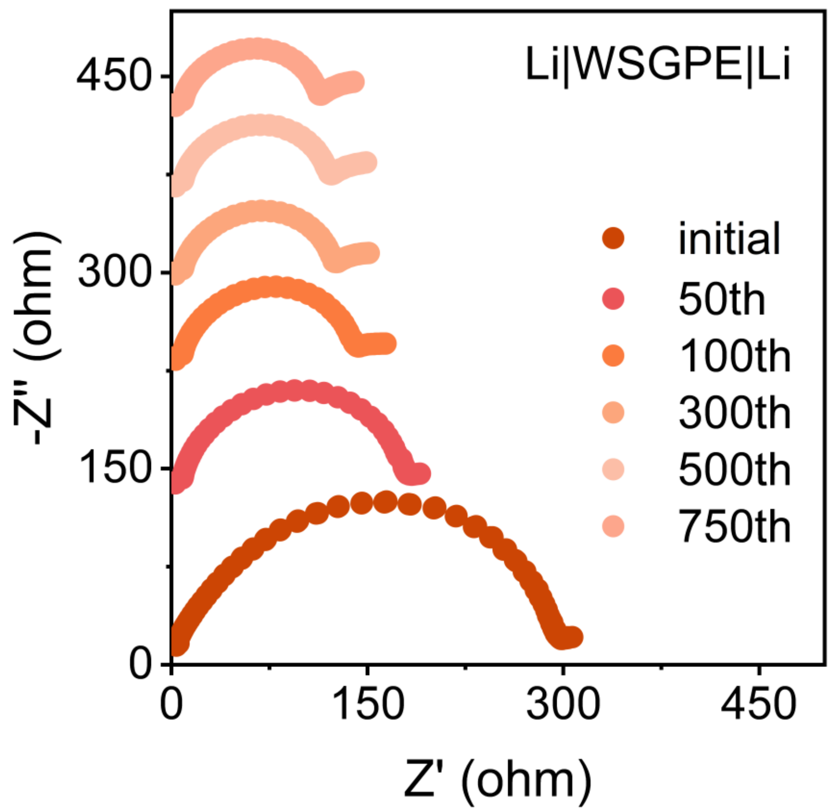

Supplementary Figure 30. Interfacial stability of the Li symmetric cell. EIS plots during cycling of Li|WSGPE|Li cell.

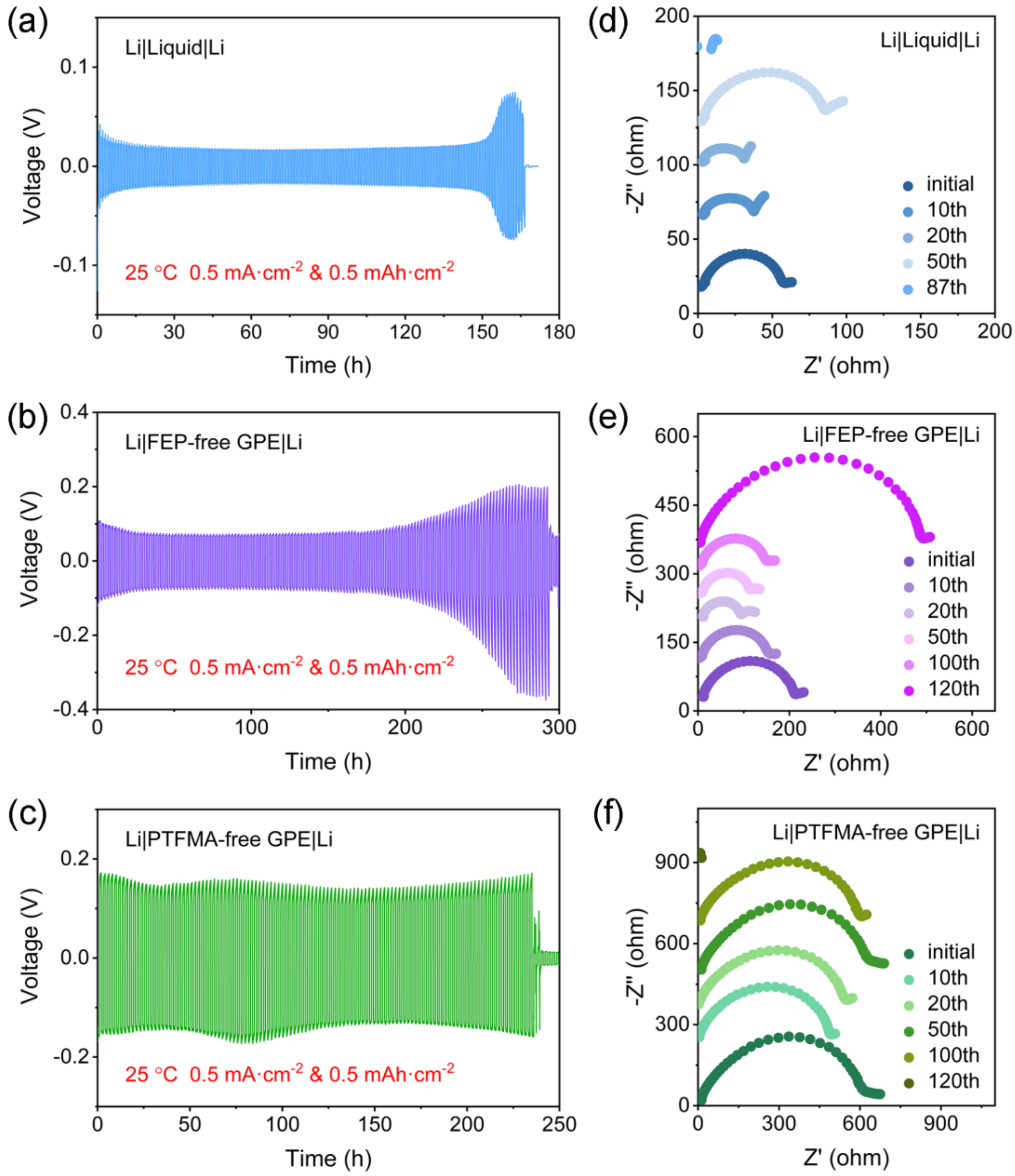

Supplementary Figure 31. Interfacial stability of Li symmetric cells with different electrolytes. Galvanostatic cycling performance of Li symmetric cells using (**a**) liquid electrolyte, (**b**) FEP-free GPE and (**c**) PTFMA-free GPE. EIS plots during cycling of Li symmetric cells using (**d**) liquid electrolyte, (**e**) FEP-free GPE and (**f**) PTFMA-free GPE.

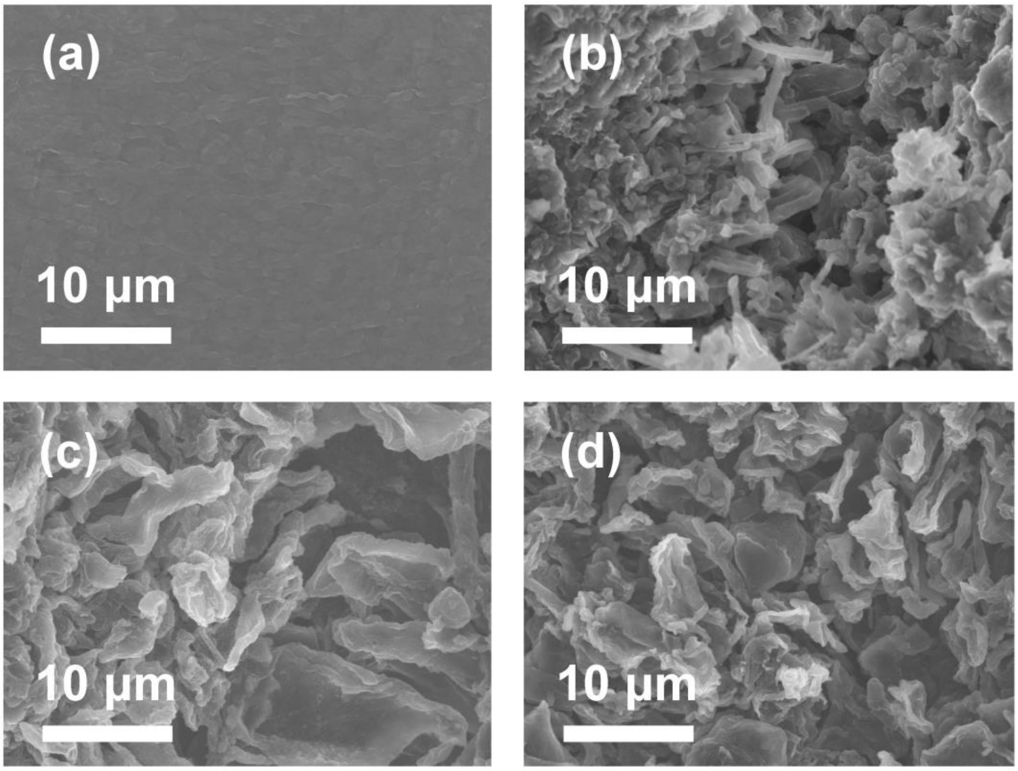

Supplementary Figure 32. Surface morphology of cycled Li. SEM images of Li from (**a**) Li|WSGPE|Li, (**b**) Li|Liquid|Li, (**c**) Li|FEP-free GPE|Li and (**d**) Li|PTFMA-free GPE|Li cells after cycling.

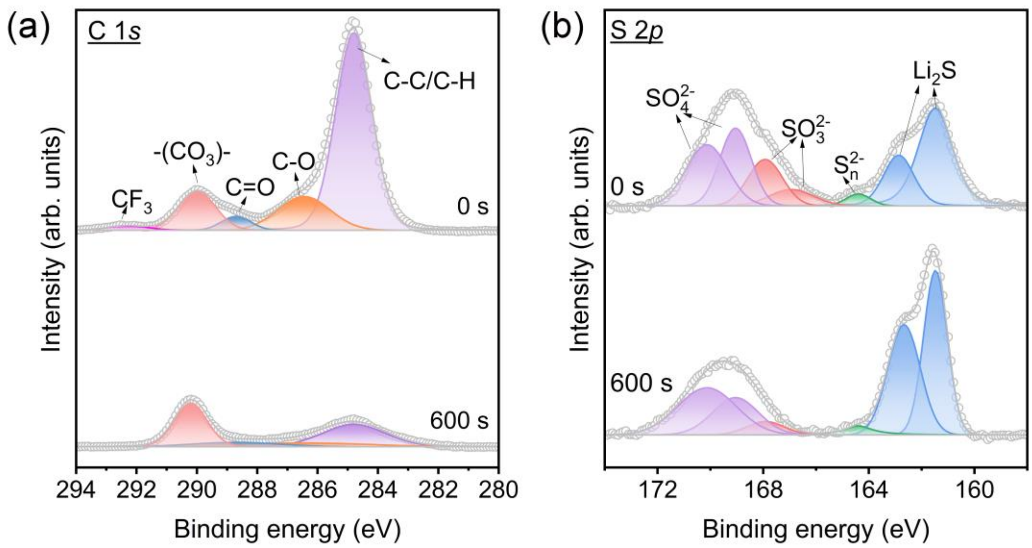

Supplementary Figure 33. The composition of SEI in WSGPE batteries. XPS depth profiles of (**a**) C 1*s* and (**b**) S 2*p* on the Li surface after 100 cycles of Li|WSGPE|Li cells at a current density of 0.5 mA cm^{-2} and an area capacity of 0.5 mAh cm^{-2}.

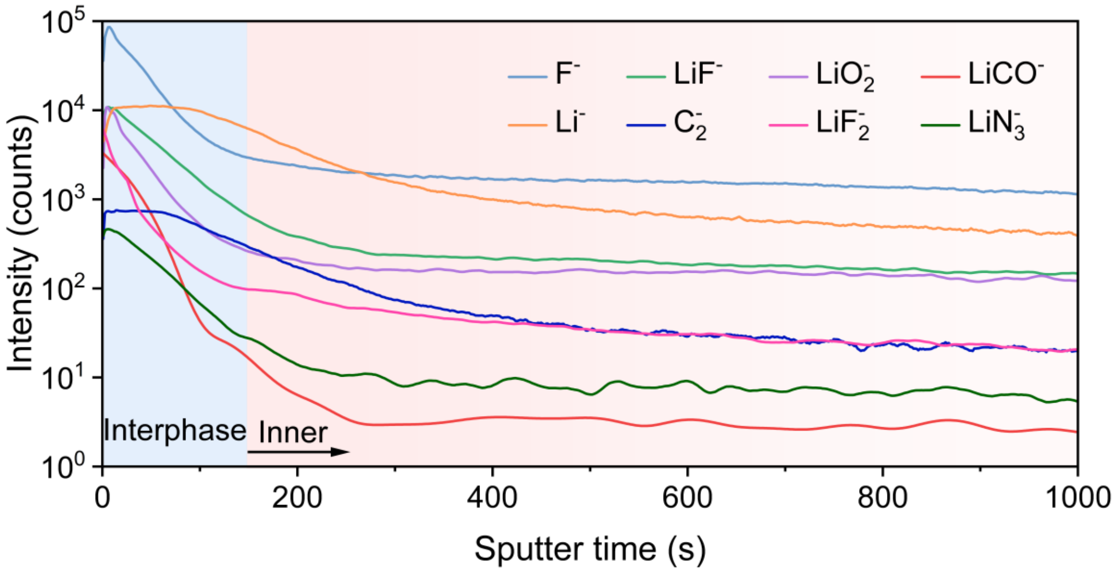

Supplementary Figure 34. The composition of SEI in WSGPE batteries. TOF-SIMS depth profiles of Li after 100 cycles in a Li|WSGPE|Li cell at a current density of 0.5 mA cm^{-2} and an area capacity of 0.5 mAh cm^{-2}.

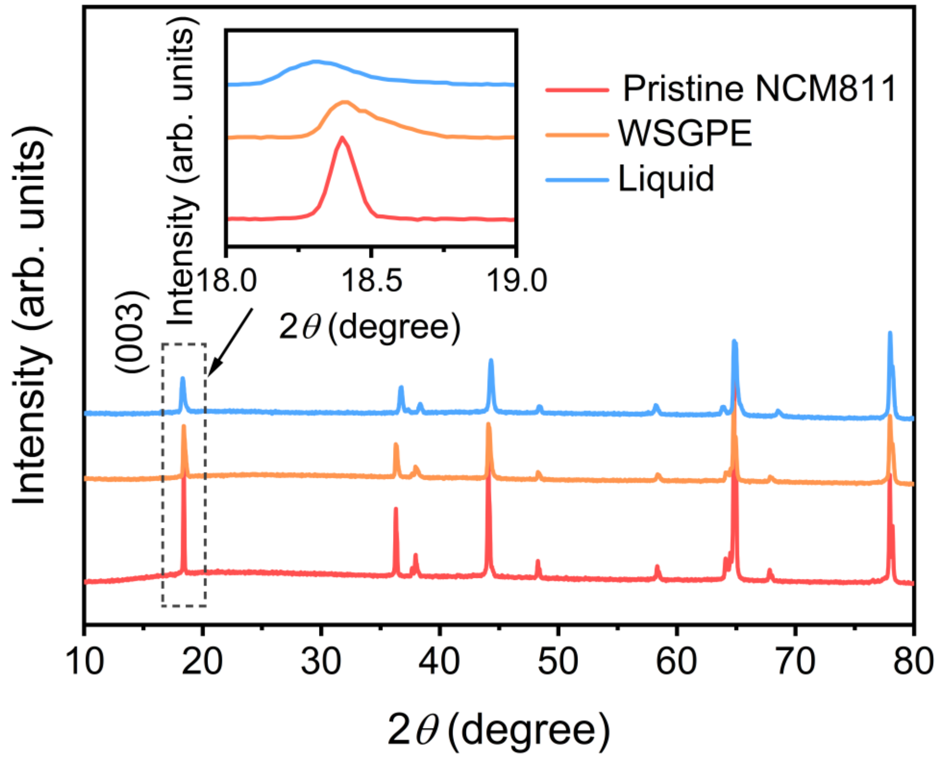

Supplementary Figure 35. The structure of NCM811. XRD results of pristine NCM811, NCM811 with WSGPE and Liquid after 100 cycles at 188 mA g^{-1}.

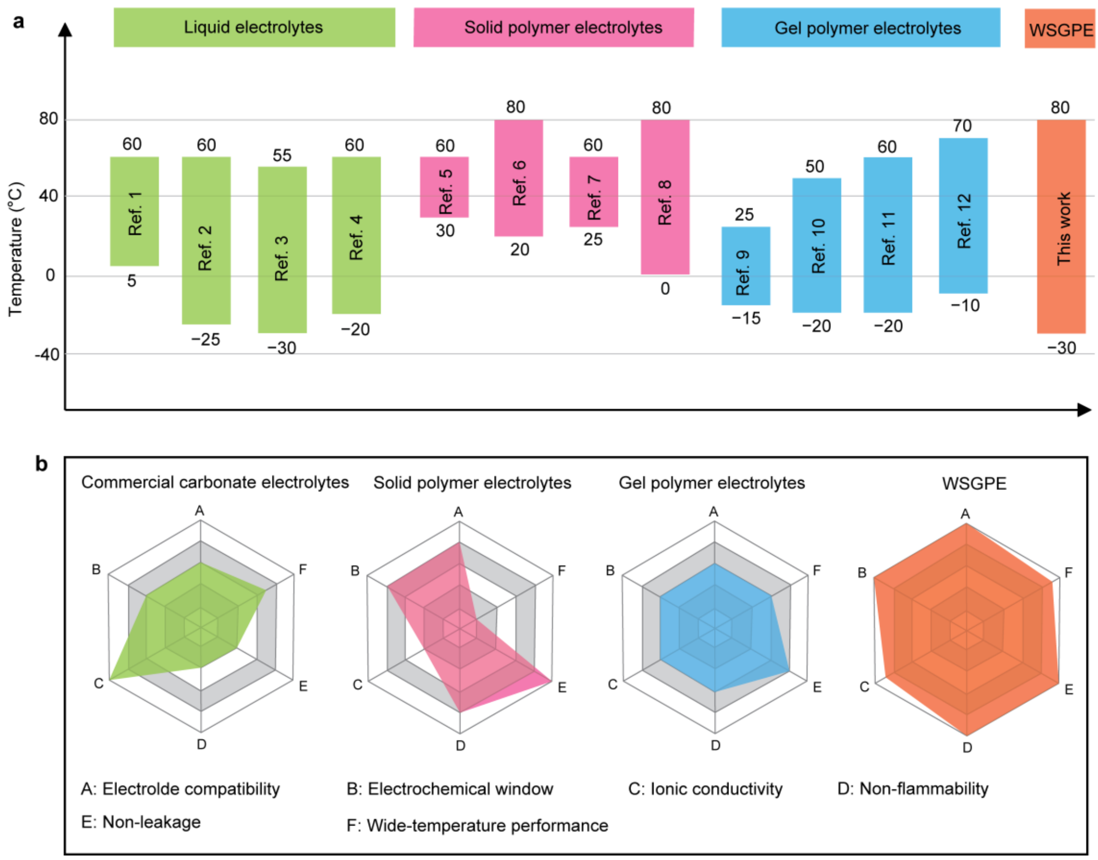

Supplementary Figure 36. Comprehensive performance of WSGPE. (**a**) Operation temperature ranges of recently reported electrolytes for Li metal batteries. (**b**) Performance comparisons of batteries with different electrolytes.

Supplementary Table 5. Summary of electrochemical properties of different electrolytes. List of representative electrolytes and their electrochemical performance in wide-temperature regions.

Electrolyte type	Electrolyte formula	Cell type	Capacity retention at LT	Capacity retention at HT	Temperature range	Refs.
LEs	1M LiFSI DME:TTE (1:2 by vol)	Li||NCM622 (2.8−4.3 V)	~95%@50 cycles@1 C@5 °C	~71%@100 cycles@C/3, 1 C (C/D)@60 °C	5−60 °C	1
	CCE-TMU/$LiNO_3$	Li||$LiFePO_4$	–	–	−25−60 °C	2
	LiFSI-DME-TTE (1:1:3 by mol)	Li||LCO (3–4.5 V)	88%@1 cycle@0.15 C@ −30 °C (charged at RT)	81.3%@200 cycles@0.7 C@55 °C	−30−55 °C	3
	PWSE + LiFMDFB + $AgNO_3$	Li||LCO (3−4.4 V)	79.3%@300 cycles@0.2 C@−20 °C	–	−20−60 °C	4
SPEs	PDOL/PLAS	Li||$LiFePO_4$	80%@400 cycles@ 3 C@30 °C	~100%@50 cycles@3 C@60 °C	30−60 °C	5
	PAN-*insitu*	Li||NCM622 (3−4.3 V)	93.7%@200 cycles@ 0.1 C@RT	60.6%@1 cycle@0.3 C@80 °C	20−80 °C	6
	LiTFSI-ADP-PEO	Li||$LiFePO_4$	99.84%@350 cycles@ 0.2 C@RT	84.1%@1000 cycles@1 C@60 °C	25−60 °C	7
	UFF/PEO/PAN/LiTFSI	Li||NCM811 (2.8−4.3 V)	~40%@1 cycle@0.1 C@0 °C	67%@150 cycles@0.1 C@50 °C	0−80 °C	8
GPEs	LiTFSI-VEC	Li||$LiFePO_4$	61%@1 cycle@ 0.1 C@−15 °C	~100%@100 cycles@1 C@RT	−15−25 °C	9
	LiTFSI/PDOL	Li||S	60%@ −20 °C	70.6%@100 cycles@0.5 C@50 °C	−20−50 °C	10
	E-QSPE	Li||$LiFePO_4$	~100%@550 cycles@0.1 C@−20 °C	80%@500 cycles@2 C@60 °C	−20−60 °C	11
	1 M LiTFSI /LiBOB in EC/PC/FEC	Li||$LiFePO_4$ (2.5−4.2 V)	41.6%@1 cycle@1 C@−10 °C	92.9%@300 cycles@1 C@70 °C	−10−70 °C	12
This work	WSPE	Li||NCM811 (3−4.3 V)	97.1%@200cycles @0.2 C@−20 °C	94%@100cycles@1 C@80 °C	−30−80 °C	

Supplementary Note 1

Interaction of components in different electrolytes and their solvation structures

In Fourier transform infrared (FTIR) spectra, the precursor of FEP-free GPE shows a distinct peak of C=C bond at 1640 cm^{-1}. After curing at 70 °C for 5 h, the C=C peak disappears obviously, indicating the complete polymerization of TFMA (Supplementary Figure 7a). The peak of the S-N-S stretching vibration of $TFSI^-$ is shown in Supplementary Figure 7b, from which can study the solvation structure of electrolytes. $TFSI^-$ in the FEC liquid electrolyte (1M LiTFSI in FEC) mainly exists in the form of free anions (FAs), and the addition of TFMA precursors has no significant effect on the solvation structure of the FEC liquid electrolyte. $TFSI^-$ anions in FEP-free GPE are also dominated by FAs. These results indicate that there is no obvious interaction between FEC and PTFMA.

As shown in Supplementary Figure 8, there is no significant difference between the solvation structures of the liquid electrolyte and the PTFMA-free GPE, which are both dominated by FAs without AGGs. In contrast, the peak of $TFSI^-$ in WSGPE shows a significant blue shift, indicating that PTFMA induces the solvation structure transition from FAs-dominated to CIPs-dominated state.

To further reveal the interactions among the components and their effects on the solvation structure, nuclear magnetic resonance (NMR) spectroscopy was performed (Supplementary Figure 9). The addition of PTFMA framework to FEC liquid electrolytes does not significantly change the ^{19}F signal of $TFSI^-$, indicating that the PTFMA polymer framework has no significant effect on the solvation structure of FEC liquid electrolytes, and that $TFSI^-$ mainly exists in the form of free groups. However, the strong interaction between PTFMA and FEP causes a significant upfield shift of the ^{19}F signal of $TFSI^-$, suggesting stronger binding of $TFSI^-$ and Li^+.

Supplementary Note 2

Cycling performance comparison of Li||NCM811 cells using different electrolytes

As shown in Supplementary Figure 13, the Li|WSGPE|NCM811 cell shows the best cycling stability, delivering a capacity of 120.8 mAh g^{-1} after 300 cycles, with an average capacity decay of only 0.087% per cycle. The liquid electrolyte and FEP-free GPE have high ionic conductivity and deliver high initial capacity of 167.8 mAh g^{-1} and 169.3 mAh g^{-1}, respectively. However, after 300 cycles, the capacity is only 51.4% and 50.5% of the initial value, respectively. The Li|PTFMA-free GPE|NCM811 cell only delivers a capacity of 63.2 mAh g^{-1} after 300 cycles, which is 43.3% of the initial capacity.

Supplementary References

1. Park, K., Jo, Y., Koo, B., Lee, H. & Lee, H. Wide temperature cycling of Li-metal batteries with hydrofluoroether dilution of high-concentration electrolyte. *Chem. Eng. J.* **427**, 131889 (2022).
2. Piao, Z. et al. Constructing a stable interface layer by tailoring solvation chemistry in carbonate electrolytes for high-performance lithium-metal batteries. *Adv. Mater.* **34**, 2108400 (2022).
3. Ren, X. et al. Designing advanced in situ electrode/electrolyte interphases for wide temperature operation of 4.5 V Li||$LiCoO_2$ batteries. *Adv. Mater.* **32**, 2004898 (2020).
4. Kim, S. et al. Wide-temperature-range operation of lithium-metal batteries using partially and weakly solvating liquid electrolytes. *Energy Environ. Sci.* **16**, 5108–5122 (2023).
5. Zhou, J. et al. High-safety all-solid-state lithium-metal battery with high-ionic-conductivity thermoresponsive solid polymer electrolyte. *Nano Lett.* **19**, 3066–3073 (2019).
6. Yao, M., Ruan, Q., Yu, T., Zhang, H. & Zhang, S. Solid polymer electrolyte with in-situ generated fast Li^+ conducting network enable high voltage and dendrite-free lithium metal battery. *Energy Storage Mater.* **44**, 93–103 (2022).
7. Han, L. et al. Flame-retardant ADP/PEO solid polymer electrolyte for dendrite-free and long-life lithium battery by generating Al, P-rich SEI layer. *Nano Lett.* **21**, 4447–4453 (2021)
8. He, F., Tang, W., Zhang, X., Deng, L. & Luo, J. High energy density solid state lithium metal batteries enabled by sub-5 µm solid polymer electrolytes. *Adv. Mater.* **33**, 2105329 (2021).
9. Lin, Z. et al. A wide-temperature superior ionic conductive polymer electrolyte for lithium metal battery. *Nano Energy* **73**, 104786 (2020).
10. Xiang, J. et al. A flame-retardant polymer electrolyte for high performance lithium metal batteries with an expanded operation temperature. *Energy Environ. Sci.* **14**, 3510–3521 (2021).
11. Ren, W. et al. In-situ formation of quasi-solid polymer electrolyte for improved lithium metal battery performances at low temperatures. *J. Power Sources* **542**, 231773 (2022).
12. Yu, J. et al. A solid-like dual-salt polymer electrolyte for Li-metal batteries capable of stable operation over an extended temperature range. *Energy Storage Mater.* **37**, 609–618 (2021).